Strategies for Wideband Light Generation in Nonlinear Multimode Integrated Waveguides

Yohann Franz, Jack Haines, Cosimo Lacava, and Massimiliano Guasoni*
Optoelectronics Research Centre, University of Southampton, Southampton SO17 1BJ, UK

In this paper we discuss two strategies to achieve wideband light generation through intermodal nonlinear parametric processes in multimode integrated waveguides. We outline how the interplay among intermodal interactions and high dispersion may lead to the generation of light characterized by substantial power spectral density if compared to supercontinuum sources. These results are valid independently of the waveguide material, however our numerical simulations focus on silicon waveguides, which are nowadays at the core of integrated photonics. The long-term vision is that, by exploiting an adequate number of intermodal processes, widely tunable radiation having high-power spectral density can be generated in a broad portion of the transparency window of silicon.

I. INTRODUCTION

Coherent optical sources and amplifiers in the near and mid-infrared (IR) spectral region are of utmost importance for several applications spanning from telecommunications up to gas sensing and medicine. Quantum cascade lasers (QCLs) are today a mature technology for light emission beyond 4 μm [1]. Rare-earth-doped silica fibers are efficient optical sources in the spectral region below 2.2 μm [2]. In these fibers light amplification occurs however in a fixed bandwidth where stimulated emission takes place. Compared with QCLs and rare-earth-doped fibers, nonlinear parametric processes represent a flexible way to generate light in broad and tunable spectral regions. Optical parametric oscillators (OPOs) based on quadratic processes in nonlinear crystals can be widely tunable in the IR [3], however they are relatively bulky systems.

In this paper we focus our attention on parametric processes based on cubic (Kerr) nonlinearity in integrated waveguides. Over the last years, parametric processes have been widely investigated in single-mode waveguides [4–15]. However, the single-mode platform is intrinsically limited: either broadband gain is achieved in the near-zero anomalous dispersion regime and close to the pump wavelength; or narrow-band gain is achieved far from the pump in the near-zero normal dispersion regime mediated by 4th-order dispersion [14–17].

Recently, researchers have started to investigate multimode waveguides [18–22], where several interactions among different spatial modes contribute to the nonlinear dynamics. These pioneering works open the way to the use of intermodal nonlinear interactions in integrated waveguides, however up to date the full potential of these interactions is far from being reached. The purpose of this work is therefore to highlight this great and still unexploited potential and some key strategies for its exploitation. Firstly, we demonstrate that, differently from single-mode waveguides, multimode waveguides may exhibit wideband parametric gain far from the pump. Secondly, we introduce the idea of concatenation of gain bands: different couples of spatial modes may give rise to several distinct parametric processes in different spectral regions that can be concatenated so as to form a single and wide gain band. In addition, we discuss how the interplay among intermodal processes and large dispersion can give rise to a radiation characterized by a relatively high power spectral density, if compared to supercontinuum sources. Despite these ideas are valid independently of the waveguide material, however in this paper our numerical simulations focus on silicon waveguides. Indeed, silicon is today the most versatile and investigated material for integrated photonics [23]. It possesses a wide transparency window of 262 THz in the near and mid-IR (from 1.1 μm to 8 μm), as well as a large nonlinear response that leads to significant nonlinear interactions over a centimeter length scale. This opens the way to fully-integrated on-chip silicon optical sources that are cheap, compact and CMOS compatible if compared with traditional OPOs.

Nevertheless, at present the largest gain bandwidth achievable in single-mode silicon waveguides and reported in literature is 20 THz, which is merely 8% of the total transparency window of silicon [13]. Therefore, the long-term vision that this paper aims to introduce is that, by exploiting an adequate number of intermodal processes, high-power spectral density radiation may be generated in a very broad bandwidth within the transparency window of silicon.

II. MODELING

As anticipated, in this paper the discussion of the main ideas is supported by the numerical simulation of silicon waveguides. We focus here on the case of free-standing (suspended) silicon rectangular waveguides: indeed, despite their fabrication is challenging, nevertheless they are currently the subject of intense research [24, 25] as they offer the opportunity to fully exploit the optical transparency window of silicon (1.1-8 μm), which otherwise would be reduced in the presence of a silica cladding.

* m.guasoni@soton.ac.uk

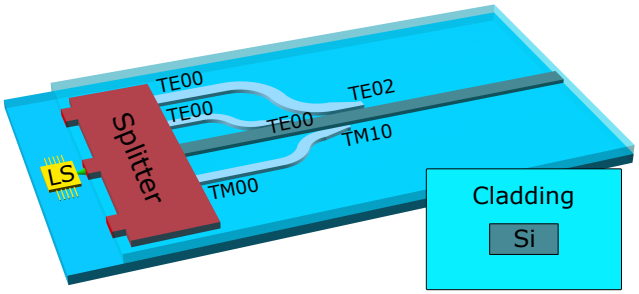

FIG. 1. Schematic setup of the system under analysis. The light from a laser source (LS) is split into several channels. In this example 3 channels are represented (directional couplers in light gray colour). The light at the input of each channel is coupled on either the fundamental TE00 or TM00 mode through the beam splitter. Each channel provides the conversion and coupling of a specific mode into the main silicon waveguide (dark gray colour). In this example, the 3 channels allows coupling into the main silicon waveguide a combination of TE02, TE00 and TM10 modes. The interaction among these modes into the waveguide gives rise to several different intermodal parametric processes that are the main topic of this paper. In the inset: cross-section representation of the main silicon waveguide.

However, it is worth noting that the main ideas discussed in this work are independent of the waveguide geometry or material, and can be therefore generalized to any kind of integrated waveguide.

The schematic setup of the system under analysis is represented in Fig.1. The light from a laser pump source is injected into a beam splitter that separates the input beam into N-channels. Each channel enables mode conversion from the fundamental mode (TE00 or TM00) to a distinct spatial mode. A control element (e.g. a modulator [26]) in each channel allows to tune the power. As a result, a linear combination of spatial modes can be injected in the waveguide. The channels could be implemented either as integrated directional couplers [26], as in Fig.1, or through external free-space phase-plates [19].

Optical pulse propagation in a silicon waveguide can be described by a set of coupled nonlinear Schrödinger equations (CNLSEs) [8, 27].

Rectangular waveguides typically exhibit large birefringence, so that only self-phase (SPM) and cross-phase modulation (XPM) are relevant to the intermodal dynamics [28], and the spatial modes are quasi-TE or quasi-TM. Consequently, the CNLSEs take the following compact form [19, 27]:

$$\frac{\partial A_n}{\partial z} = P_n - \frac{1}{2}\alpha_n A_n + i\sum_k b_{kn} C_{kn} |A_k|^2 A_n + R_n \quad (1)$$

In Eq.(1) $A_n(z,t)$ is the slowly-varying envelope of mode n. The term $P_n(z,t)$ represents the modal dispersion related to mode n. In our simulations, we model the dispersion as $P_n(z,t) = i\int_f df \beta_n(f+f_p)\hat{A}_n(z,f)exp^{-i2\pi ft}$, where f_p is a reference frequency (typically the pump frequency), $\hat{A}_n$ indicates the Fourier transform of A_n(z,t) whereas $\beta_n(f+f_p)$ is the propagation constant of mode n at the frequency $f+f_p$. This integral version of the linear dispersion implicitly takes into account for all higher-order dispersion terms, and is therefore useful when the simulation span a wide spectral band [30]. Alternatively, one may employ the usual truncated Taylor series expansion that includes a finite number of higher-order dispersion coefficients [29]. The coefficients b_{kn} account for self and cross-phase modulation and depend on the direction along which the waveguide is fabricated [8]. For common silicon waveguides fabricated along the [0 1 0] direction b_{kn}=1 if $k = n$; b_{kn}=2 if $k \neq n$ and the modes have same polarization; b_{kn}=1/2 if $k \neq n$ and the modes have orthogonal polarization [9]. The nonlinear coefficients read $C_{kn} = n_2 2\pi f_p/(cA_{eff,kn})$, where n_2 is the nonlinear refractive index of silicon at the reference frequency f_p, whereas $A_{eff,kn}$ is the effective area calculated as the overlap integral among the modal distributions $M_{k,n}(x,y)$ of modes k and n [27]. The effective areas, along with the propagation constants, are computed through a finite-element-solver taking into account for the material dispersion [31]. The coefficient α_n accounts for the linear absorption losses of mode n. The term R_n includes the Raman contribution as described in Refs.[9, 32]. We point out that both the nonlinear coefficients and the modal distributions are calculated at the reference frequency f_p, which is typically the pump frequency.We neglect therefore nonlinear dispersion. This choice is justified by the fact that it does not play any significant role in the phase-matching condition of intermodal parametric processes [28]. We also ignore two-photon absorption (TPA) and free-carrier absorption (FCA) because, as discussed in the next sections, they do not affect the dynamics in our simulations. We focus now on the parametric amplification process triggered by a pump source which is distributed over a set of spatial modes at the waveguide input (Fig.1). The simultaneous interaction between several modes into the waveguide may exhibit a complex dynamics [28]. However, its description is simplified whenever the phase-matching between each couple of modes is achieved in distinct spectral bands. In this last case the parametric amplification can be separated into a set of independent parametric processes, each one related to a distinct couple of modes n and m. In each process two photons from the pump, centred at frequency f_p and coupled over the modes n and m, are converted to one photon at frequency f_i in the Stokes side coupled to mode m and one photon at frequency f_s in the anti-Stokes side coupled to mode n, with $f_s + f_i = 2f_p$ to satisfy energy conservation [34]. Light is therefore generated at both f_s and f_i, or amplified if a wave is pre-existing at these frequencies. Moreover, maximum optical gain is achieved for those frequencies $f_{s,i}$ that satisfy the phase-matching condition:

$$\beta_n(f_p) + \beta_m(f_p) - \beta_n(f_s) - \beta_m(f_i) = 0 \quad (2)$$

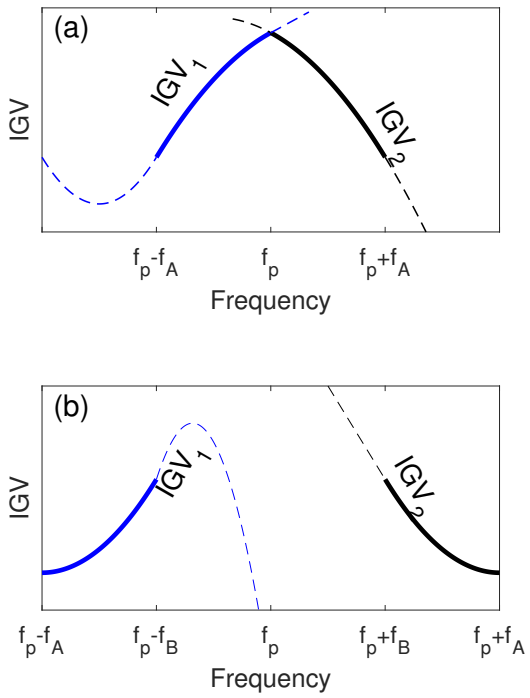

FIG. 2. Panel (a): representation of mirror symmetry around the pump, as in Ref.[35]. The inverse group velocities IGV_1 and IGV_2 of two distinct spatial modes m_1 and m_2 have mutual mirror symmetry centred at f_p and in the spectral region from $f_p - f_A$ to $f_p + f_A$ (solid lines). Outside this region the symmetry is lost (dotted lines). Consequently, effective parametric amplification of mode m_1 can be achieved for frequencies from $f_p - f_A$ to f_p, and of mode m_2 for frequencies from f_p to $f_p + f_A$.Panel (b): representation of mirror symmetry far from the pump. The inverse group velocities IGV_1 and IGV_2 of two distinct spatial modes m_1 and m_2 have mutual mirror symmetry centred at frequency f_p but far from it. In this example, efficient parametric amplification of mode m_1 is achieved for frequencies from $f_p - f_A$ to $f_p - f_B$, and of mode m_2 for frequencies from $f_p + f_B$ to $f_p + f_A$.

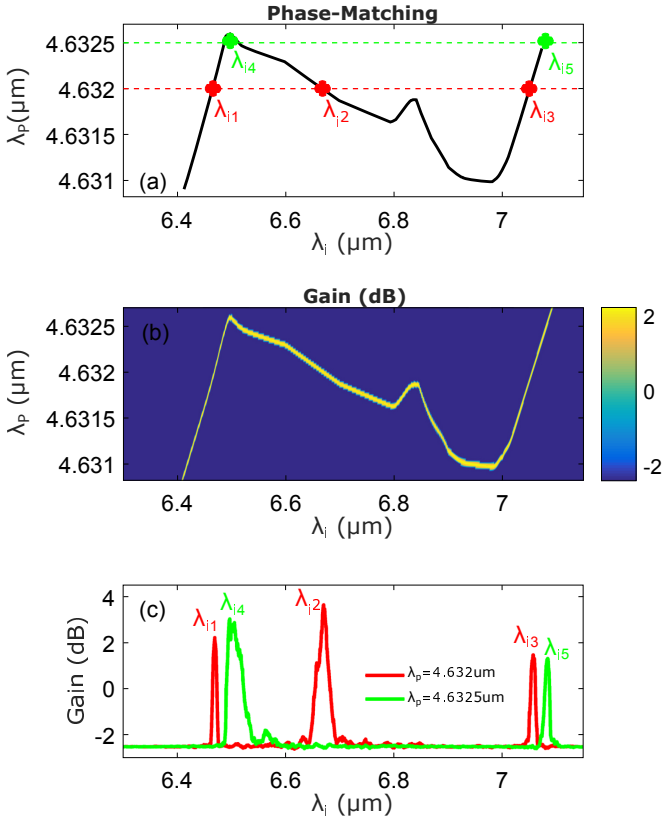

FIG. 3. Results for the 1.4x1 μm waveguide. In these simulations we set the linear losses to 0.5 dB/cm [8] for each mode and $n_2 = 3.5{\cdot}10^{-18}\ m^2/W$, which is the nonlinear index of silicon at $\sim 4.63\ \mu$m [36]. The waveguide is 5 cm long.Note that since the anti-Stokes gain band and the Stokes gain band are symmetric to each other with respect to the pump frequency, here and in the following figures we do not represent the anti-Stokes side. Panel (a): solution of the phase-matching condition Eq.(2) in the (λ_p, λ_i) plane. The horizontal dashed red and green lines indicate the pump wavelengths 4.632 and 4.6325 μm, crossing the phase-matching line at the Stokes wavelengths $\lambda_{i1,i2,i3,i4,i5}$. Panel (b): surface plot of the net gain at the waveguide output in the (λ_p, λ_i) plane, computed from solution of Eq.(1). Panel (c): net gain profile when λ_p= 4.632 μm (red line) and 4.6325 μm (green line), respectively. Negative values of gain are due to losses.

III. STRATEGY 1: MIRROR SYMMETRY OF INVERSE GROUP VELOCITIES FAR FROM THE PUMP

In this section, we illustrate a strategy to achieve wideband light generation far from the pump, thus overcoming one of the main limits of single-mode waveguides. We have recently discussed in Ref. [35] that whenever two modes have inverse group velocities exhibiting mirror symmetry around the pump frequency f_p, then the phase-matching Eq.(2) is fulfilled over a large spectral band in proximity of the pump, which leads to effective parametric amplification in that band (Fig.2(a)). Here, differently from Ref.[35], we relax the assumption of symmetry around the pump: mirror symmetry can be achieved in two bands far from the pump, which still would lead to effective phase-matching and then parametric amplification, as displayed in Fig.2(b).

By computing the inverse group velocities related to the modes of several rectangular silicon waveguides with height and width ranging from 0.7 μm to 4 μm, we found that the modes TE00 and TE01 of a waveguide with cross-section 1.4x1.0 μm exhibit quasi-mirror symmetry in the Stokes band 6.40-7.10 μm (mode TE00) and the corresponding anti-Stokes band 3.43-3.62 μm (mode TE01) , with central wavelength 4.6315 μm. Therefore, having a pump coupled to both modes TE00 and TE01 and centred at $\lambda_p = c/f_p$=4.6315 μm, effective phase-matching is expected in both the bands 6.40-7.10 μm (for mode TE00) and 3.43-3.62 μm (for mode TE01).It is worth noting that the waveguide dimensions allow

tuning the wavelengths of interest: as a general rule of thumb, by increasing (decreasing) the waveguide size we red-shift (blue-shift) the wavelength λ_p as well as the Stokes and anti-Stokes bands.

Figure 3a shows the solution of the corresponding phase matching condition Eq.(2) as a function of the pump (λ_p) and the Stokes (λ_i) wavelengths. As expected, due to the mirror-symmetry, phase matching occurs over a large bandwidth. Note that since the symmetry is not perfect (it is a quasi-mirror symmetry), a slightly tunable pump rather than a fixed wavelength one should be employed. The main outcome is that by tuning the pump wavelength λ_p in a range as narrow as 21 GHz (4.631-4.6325 μm), phase-matching, and then light generation, is achieved in the whole Stokes band 6.40-7.10 μm and the anti-Stokes counterpart 3.43-3.62 μm (9.24 THz total bandwidth), coupled respectively to the modes TE00 and TE01. For comparison, the typical gain bandwidth far from the pump mediated by fourth-order dispersion in single-mode waveguides is fractions of THz [14, 15], which is one order of magnitude smaller than in our example.

In Fig. 3b the optical gain spectrum is displayed, which is obtained from the numerical solution of Eq.(1) with an input pump coupled over the TE00 and TE01 modes and having 5 W peak-power, to which a weak background white noise is added to seed the parametric amplification process (see the figure caption for more details). The temporal walk-off over the waveguide length (L=5 cm) due to the differential group velocity among TE00 and TE01 modes is of the order of hundreds of picoseconds, which imposes the use of CW or pulsed sources with pulse width $>$ 1 ns. Note that TPA and FCA in silicon are negligible for input pump wavelengths beyond 2.2 μm [9], which is the case in this example. Moreover, stimulated Raman scattering does not occur with TE modes since the waveguide is fabricated along the [0 1 0] direction [32]. The results in Fig.3b,c confirm that by tuning the pump from 4.631 to 4.6325 μm, light can be generated continuously in the 6.40-7.10 μm spectral region as well as in the anti-Stokes counterpart 3.43-3.62 μm (here not illustrated). For example, if the pump is centred at 4.632 μm (indicated by the horizontal red dashed line in Fig.3a), then the phase-matching condition is achieved at 3 Stokes wavelengths $\lambda_{i1,i2,i3}$ (red dots in Fig. 3a). Consequently, the optical gain spectrum shows 3 peaks in correspondence of $\lambda_{i1,i2,i3}$ (see Fig.3c). If the pump is now centred at another wavelength, for example 4.6325 μm (green dotted line in Fig 3a), light is generated at different wavelengths $\lambda_{i4,i5}$. It should be noted that, besides the essential phase-matching requirement, light generation can be achieved only when the pump power exceeds a certain threshold such that net gain is obtained. Such a threshold depends on the waveguide parameters and can be well estimated through the analytical tools introduced in Ref.[28].

At variance with single-mode waveguides, where near-zero dispersion is a requisite for efficient parametric amplification, the mirror-symmetry condition does not imply any constraint on the dispersion of the modes. Consequently, the intermodal parametric amplification is efficient even in the presence of large dispersion. At the same time, a large dispersion reduces substantially the SPM-induced spectral broadening as well as the cascading of four-wave-mixing bands, and so ultimately the supercontinuum generation. This simultaneous interplay among efficient intermodal amplification and supercontinuum suppression represents a key-distinguishing feature of intermodal processes, which can be exploited for the generation of high power spectral density over a wide band. Figure 4 displays the pump-to-idler conversion and the spectral evolution of light for different waveguide lengths when a pump centred at 4.632 μm and with 35 W peak-power is injected. As expected from Fig.3, a peak of conversion is found at 6.65 μm (see black arrows in Fig. 4b,c) . Despite the formation of an underlying supercontinuum (6.2- 7.1 μm) induced by the high pump power, however this peak dominates the pump-to-idler conversion due to the large dispersion at both pump and idler wavelengths: for a length L = 6 cm, a large fraction ($\sim$ 17 %) of the total output optical power is contained in a band as narrow as 2 nm (6.649-6.651 μm, see Fig. 4 a).

Similarly to the previous example of Fig.3, the peak of conversion can be shifted by tuning the pump wavelength in the range 4.631- 4.6325 μm. As a result, differently from supercontinuum sources where the output power is spread over a broad spectral region resulting in low-power spectral density, here we can selectively allocate a substantial portion of the output power ($\sim$ 10-20 %) in a few-nm bandwidth within the spectral region extending from 6.4 to 7.1 μm. Light having high-power spectral density is therefore generated with wideband tunability, which can be of utmost importance for several applications (e.g. remote sensing). From another perspective, by quantifying the temporal coherence in terms of the radiation bandwidth as it is usually done in the case of optical sources (narrow linewidth means high temporal coherence and vice-versa), we can say that light generated through intermodal nonlinear processes exhibits a substantial temporal coherence if compared to supercontinuum radiation.

IV. STRATEGY 2: CONCATENATION OF GAIN BANDS

A second strategy to achieve wideband light generation is based on the concatenation of several spectral regions where distinct couples of modes are phase-matched. This idea is illustrated in Fig.5 and explored in Fig.6a, which refers to a waveguide with a cross-section of 1.2x1.0μm. For this specific waveguide geometry, the phase-matching points related to the couples of modes TE00-TM00,

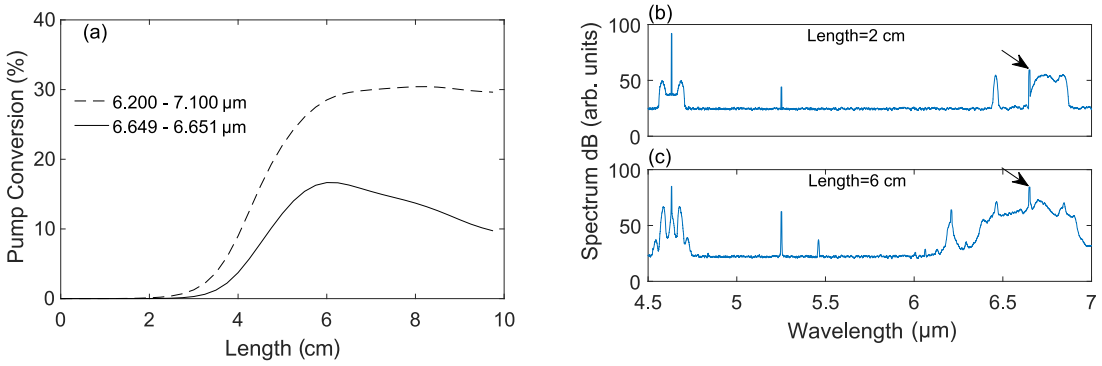

FIG. 4. Panel (a): pump-to-idler conversion as function of the waveguide length L when injecting a pump with 35 W peak-power centred at 4.632 μm. The conversion represents the ratio between the power in a given band and the total output power. Here the bands under analysis are 6.2-7.1 μm and 6.649-6.651 μm. When $L = 6$ cm about 30% of the output power is in the band 6.2-7.1 μm, a large portion of which (17%) in the narrow band 6.649-6.651 μm. Panels (b,c) illustrate the output spectrum for mode TE00: the difference between the peak centred at 6.65 μm (indicated by the black arrows) and the underlying supercontinuum exceeds 20 dB.

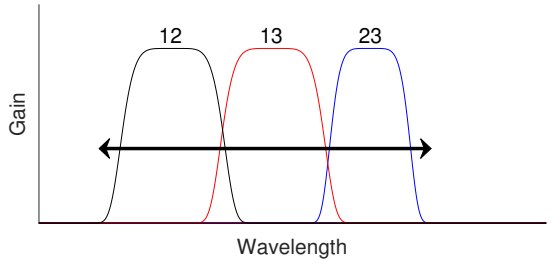

FIG. 5. Illustration of concatenation of spectral regions. An example related to 3 spatial modes m_1,m_2 and m_3 is displayed. Three distinct gain bands are present (blue, red and black lines) that are related to the intermodal processes among the different couples of modes (here indicated with 12,13,23). Typically, these bands are separated. However, for a proper waveguide design, they can be concatenated so as to form a single and continuum band (indicated by the double-arrow) where light can be generated.

.

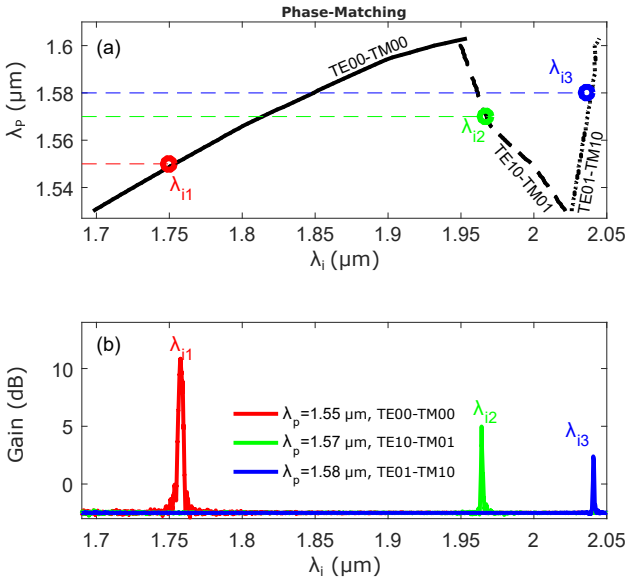

FIG. 6. Results for the 1.2x1 μm waveguide. We set linear losses to 0.5 dB/cm [8] for each mode and $n_2 = 5{\cdot}10^{-18}\ m^2/W$, which is the nonlinear index of silicon at ~ 1.55 μm [36]. The waveguide is 5 cm long. Panel (a): phase-matching lines for 3 different couples of modes: TE00-TM00 (solid line); TE10-TM01 (dashed line); TE01-TM10 (dotted line). In this specific waveguide, the 3 phase-matching lines are concatenated and cover the band 1.69-2.05 μm. The horizontal dashed blue, green and red lines indicate the pump wavelengths 1.58, 1.57 and 1.55 μm and cross the phase-matching lines at the Stokes wavelengths $\lambda_{i1,i2,i3}$. Panel (b): gain spectra for 3 different input pump configurations. Raman gain spectra have been filtered out for the sake of clarity.

TE10-TM01 and TE01-TM10 turn out to be concatenated. Specifically, modes TE00-TM00 lead to phase matching in the band 1.69-1.94 μm; modes TE10-TM01 in the band 1.94-2.02 μm ; and finally modes TE01-TM10 in the band 2.02-2.05 μm. Finally phase matching, and then parametric amplification, is achieved in the whole spectral region 1.69-2.05 μm (as well as its anti-Stokes counterpart 1.23-1.40 μm). Note however that an input tunable pump from 1.53 to 1.60 μm (10 THz) is required. For example, if the pump is centred at 1.55 μm (horizontal red dashed line in Fig.6a) and is coupled over both the TE00 and TM00 modes, then phase matching is satisfied at the Stokes wavelength $\lambda_{i1} \sim 1.76$ μm (mode TE00), represented by a red circle in Fig.6a, and the corresponding anti-Stokes wavelength $\lambda_{s1} \sim 1.38$ μm (mode TM00,not illustrated in Fig.6). Consequently, a gain peak can be observed both at λ_{i1}=1.76 μm (related to mode TE00, see the output spectrum of Fig.6b) and at the corresponding anti-Stokes wavelength λ_{s1}=1.38 μm (related to mode TM00). Similarly, if the pump is centred at 1.57 μm (horizontal green dashed line in Fig.6a)

and is coupled over the TE10 and TM01 modes, phase-matching is satisfied at λ_{i2}=1.97 μm (mode TE10, see green circle in Fig.6a and the corresponding gain spectrum in Fig.6b) and at the corresponding anti-Stokes wavelength $\lambda_{s2} \sim 1.30$ μm (mode TM01). It is worth noting that the largest gain bandwidth achieved in single-mode waveguides up to date is $\sim$ 20 THz [13]. It could raise up to $\sim$ 30 THz when using a pump tunable over 10 THz, which is however only half the bandwdith achieved in this example. Similarly to the example in the previous section, this demonstrates one time more the great potential and flexibility offered by intermodal interactions. Interesting enough, in this specific example commercial erbium-doped fiber lasers (EDFLs) would represent an ideal input pump source, as they cover the 1.53-1.60 μm spectral region (telecom band). In this band, silicon suffers from high TPA and FCA. However, when the pump pulse width T_{pulse} is much shorter than the effective carrier lifetime T_{FCA}, then FCA and TPA are negligible [8] and Eq.1 can be employed. Note that in practice T_{FCA} can be controlled either by applying an external direct current or by properly designing the waveguide cross-section [9], so that it may vary from less than 1 nanosecond to tens of nanoseconds. We solve therefore Eq.1 under the assumption that $T_{pulse} << T_{FCA}$. Figure 6b shows the gain when the pump peak-power is 6 W and for different input pump configurations. By properly coupling the pump over the couples of modes previously discussed, net gain is achieved in the whole spectral region $1.69 - 2.05\mu$m.

V. CONCLUSION

In this paper we have discussed two effective strategies to achieve wideband light generation in multimode integrated waveguides through the exploitation of intermodal nonlinear Kerr-processes. By properly optimizing the waveguide geometry we can exploit the mirror-symmetry principle or concatenate the phase-matching bands related to different couples of modes in such a way to cover a wide, continuous band where light can be generated with high power spectral density and temporal coherence if compared to supercontinuum sources. These strategies disclose the great potential of intermodal processes, which is still unexploited so far.
We stress that the numerical simulations discussed in this paper depend on the linear and nonlinear parameters that are used to model the waveguide through Eq.1. These parameters, however, cannot be determined a priori with exactness, since they are affected by the deposition steps at fabrication stage, which explains why different values may be found in literature [37, 38]. This is all the more true when simulating over large spectral regions. Therefore, the numerical results displayed in Figs.3,6 should be intended as a guideline to illustrate the substantial potential of the two strategies introduced in this paper, rather then a definitive design of optimal waveguide geometries and an accurate characterisation of their performance.
Finally, we highlight that the main ideas illustrated in this work can be generalized to any kind of waveguide geometry and materials. The preliminary results discussed in this work should therefore stimulate the investigation of more complex strategies (e.g. simultaneous mirror-symmetry and concatenation), geometries (e.g. coupled waveguides) or multi-pump configurations that would offer more degrees of freedom for an optimal design of the phase-matching conditions, ultimately leading to light generation in a very wide IR band.

FUNDING

This research is funded by the European Research Council under Grant Agreement No.802682 -ERC Starting Grant MODES.

ACKNOWLEDGMENTS

The authors are grateful to Dr. M.Passoni for useful discussions.

[1] Y. Yao, A.J. Hoffman, C.F. Gmachl, "Mid-infrared quantum cascade lasers" , Nature Phot.**6**,432 (2012)
[2] D. J. Richardson, J. Nilsson, W. A. Clarkson, "High power fiber lasers: current status and future perspectives [Invited]," J. Opt. Soc. Am. B **27**,B63 (2010)
[3] J. Armougom, Q. Clément , J.-M. Melkonian,J.-B. Dherbecourt , M. Raybaut ,A. Grisard , E. Lallier , B. Gérard,B. Faure , G. Souhaité , A. Godard,"Single-frequency tunable long-wave infrared OP-GaAs OPO for gas sensing", SPIE LASE, 2017, San Francisco, California, United States, 100880Z (2017)
[4] J. Leuthold, C. Koos and W. Freude," Nonlinear silicon photonics",Nature Phot.**4**,535 (2010)
[5] M. Lamy, C. Finot, P. Colman, J. Fatome, G. Millot, G. Roelkens, B. kuyken, K. Hammani , "Silicon Waveguides for High-Speed Optical Transmissions and Parametric Conversion Around 2 μm," in IEEE Phot. Tech. Letters **31**,165 (2019)
[6] R.Soref, "Mid-infrared photonics in silicon and germanium", Nature Phot.**4**,495 (2010)
[7] L. Razzari, D. Duchesne, M. Ferrera, R. Morandotti, S. Chu, B. E. Little, D. J. Moss, "CMOS-compatible integrated optical hyper-parametric oscillator", Nature Phot.**4**,41 (2010)
[8] Q. Lin,J.Zhang,P.Fauchet, G. P. Agrawal, "Ultrabroadband parametric generationand wavelength conversion in

silicon waveguides", Opt. Expr.**14**,4786 (2006)
[9] Q. Lin,J.Zhang,O,J.Painter, G. P. Agrawal, "Nonlinear optical phenomena in silicon waveguides: modeling and applications", Opt. Expr.**15**,16604 (2007)
[10] S.Azzini, D. Grassani, M.Galli, L.C.Andreani, M.Sorel, M.J.Strain, L. G. Helt, J. E. Sipe, M.Liscidini, and D.Bajoni, "From classical four-wave mixing to parametric fluorescence in silicon microring resonators", Opt. Lett.**37**,3807 (2012)
[11] C. Lacava, M. J. Strain, P. Minzioni, I. Cristiani, and M. Sorel "Integrated nonlinear Mach Zehnder for 40 Gbit/s all-optical switching", Opt. Lett.**21**,21587 (2013)
[12] M. Strain, C. Lacava, L. Meriggi, I. Cristiani, and M. Sorel, "Tunable Q-factor silicon microring resonators for ultra-low power parametric processes", Opt. Lett.**40**,1274 (2015)
[13] B. Kuyken et al."On-chip parametric amplification with 26.5 dB gain at telecommunication wavelengths using CMOS-compatible hydrogenated amorphous silicon waveguides", Opt. Lett. **36**,552 (2011)
[14] B.Kuyken,X.Liu,R.M. Osgood Jr., R.Baets, G.Roelkens, W.M.J.Green, "Mid-infrared to telecom-band supercontinuum generation in highly nonlinear silicon-on-insulator wire waveguides," Opt. Express **19**,20172 (2011)
[15] B.Kuyken,X.Liu,R.M. Osgood Jr., R.Baets, G.Roelkens, W.M.J.Green,"A silicon-based widely tunable short-wave infrared optical parametric oscillator",Opt. Express **21**,5931 (2013)
[16] A.Picozzi, G.Millot, and S.Wabnitz, "Nonlinear optics: Nonlinear virtues of multimode fibre," Nature Phot. **9**,289 (2015).
[17] K. Krupa,A.Tonello, et al. "Spatial beam self-cleaning in multimode fibres", Nature Photonics, **11**,237 (2017)
[18] S.Signorini, M. Mancinelli, M. Borghi, M.Bernard, M.Ghulinyan, G.Pucker, L. Pavesi,"Intermodal four-wave mixing in silicon waveguides", Phot.Research **6**,805 (2018)
[19] C. Lacava et al.,"Intermodal Bragg-Scattering Four Wave Mixing in Silicon Waveguides", J. Light.Technology **37**,1680 (2019)
[20] Y. Zhao, et.al,"Visible nonlinear photonics via high-order-mode dispersion engineering", Optica **37**,135 (2020)
[21] C. Lacava, T. Dominguez Bucio, A. Z. Khokhar, P. Horak, Y. Jung, F. Y. Gardes, D. J. Richardson, P. Petropoulos, and F. Parmigiani, "Intermodal frequency generation in silicon-rich silicon nitride waveguides," Photon. Res. **7**,615 (2019)
[22] B.N.Carnio and A. Y. Elezzabi, "Backward terahertz difference frequency generation via modal phase-matching in a planar LiNbO3 waveguide," Opt. Lett. **45**,3657 (2020)
[23] D. Thomson et al.,"Roadmap on silicon photonics", J. of Optics **18**,073003 (2016)
[24] J.S. Penades et al., "Suspended silicon waveguides for long-wave infrared wavelengths", Opt. Lett. **43**,795 (2018)
[25] R., T.Hatakeyama, J.Horng, J.H.Kang, Y. Wang, X.Zhang, and F. Wang, "Mid-IR broadband supercontinuum generation from a suspended silicon waveguide", Opt. Lett. **43**,1387 (2018)
[26] D.Dai, J.Wang, and Y. Shi, "Silicon mode (de)multiplexer enabling high capacity photonic networks-on-chip with a single-wavelength-carrier light", Opt. Lett.**38**,1422 (2013)
[27] A.Peacock,P.Metha,P.Horak,N.Heady, "Nonlinear pulse dynamics in multimode silicon core optical fibers", Opt. Lett.**37**,3351 (2012)
[28] M.Guasoni, "Generalized modulational instability in multimode fibers: Wideband multimode parametric amplification", Phys.Rev.A **92**,033849 (2015)
[29] F. Poletti and P. Horak, "Description of ultrashort pulse propagation in multimode optical fibers," J. Opt. Soc. Am. B **25**,1645 (2008)
[30] B. Kuyken, P. Verheyen, P. Tannouri, X. Liu, J. Van Campenhout, R. Baets, W. M. J. Green, and G. Roelkens, "Generation of 3.6 μm radiation and telecom-band amplification by four-wave mixing in a silicon waveguide with normal group velocity dispersion," Opt. Lett. **39**,1349 (2014)
[31] H. H. Li, "Refractive index of silicon and germanium and its wavelength and temperature derivatives", J. Phys. Chem. Ref. Data **9**,561 (1980)
[32] A. Liu, H. Rong, R. Jones, O. Cohen, D. Hak, and M. Paniccia, "Optical amplification and lasing by Stimulated Raman Scattering in Silicon Waveguides", J. of Light. Technology **24**,1440 (2006)
[33] C.Lacava, S. Stankovic, A. Z. Khokhar, T. D.Bucio, F. Y. Gardes, G. T. Reed, D.J. Richardson , P. Petropoulos , "Si-rich Silicon Nitride for Nonlinear Signal Processing Applications", Sci.Reports**7**,1 (2017)
[34] G. P. Agrawal, "Nonlinear Fibre Optics, 4th Edition", Elsevier (2007)
[35] M.Guasoni, F.Parmigiani, P.Horak, D.J. Richardson, " Novel fiber design for wideband conversion and amplification in multimode fibers" in 2017 European Conference on Optical Communication (ECOC). vol. 2017-September, IEEE, 1-3 (2017)
[36] L.Zhang,A. M. Agarwal, L.C. Kimerling, J. Michel, "Nonlinear Group IV photonics based on silicon and germanium: from near-infrared to mid-infrared", Nanophotonics**3**,247 (2014)
[37] C.Lacava,M.A.Ettabib,P. Petropoulos, "Nonlinear silicon photonic signal processing devices for future optical networks", Applied Sciences**7**,103 (2017)
[38] A.D. Bristow, N. Rotenberg, H.M. Van Driel," Two-photon absorption and Kerr coefficients of silicon for 850-2200 nm", Appl. Phys. Lett.**90**,191104 (2007)